

Single layer of MX₃ (M=Ti, Zr; X=S, Se, Te): a new platform for nano-electronics and optics

Yingdi Jin,^a Xingxing Li^a and Jinlong Yang^{*a,b}

Received (in XXX, XXX) Xth XXXXXXXXXX 20XX, Accepted Xth XXXXXXXXXX 20XX

DOI:

A series of two dimensional titanium and zirconium trichalcogenides nanosheets MX₃ (M=Ti, Zr; X=S, Se, Te) are investigated based on first-principles calculations. The evaluated low cleavage energy indicates that stable two dimensional monolayers can be exfoliated from their bulk crystals in experiment. Electronic studies reveal very rich electronic properties in these monolayers, including metallic TiTe₃ and ZrTe₃, direct band gap semiconductor TiS₃ and indirect band gap semiconductors TiSe₃, ZrS₃ and ZrSe₃. The band gaps of all the semiconductors are between 0.57~1.90 eV, which implies their potential applications in nano-electronics. And the calculated effective masses demonstrate highly anisotropic conduction properties for all the semiconductors. Optically, TiS₃ and TiSe₃ monolayers exhibit good light absorption in the visible and near-infrared region respectively, indicating their potential applications in optical devices. In particular, the highly anisotropic optical absorption of TiS₃ monolayer suggests it could be used in designing nano optical waveguide polarizers.

Introduction

Since the successful isolation of graphene,¹ two dimensional (2D) materials have attracted tremendous attentions with a wide range of physicochemical properties and potential applications. Pristine graphene lacks a finite band gap, which is essential for controllable and reliable transistor operation. Thus, for nano-electronics and optics, it is necessary to explore other two dimensional materials²⁻¹² with suitable band gaps, for example transition metal dichalcogenides⁵⁻⁷ and the recently rediscovered phosphorene.⁸⁻¹² Moreover, benefited from the state-of-art liquid exfoliation method,¹³⁻¹⁵ it is now possible to extract single layered materials from any van der Waals (vdW) stacked layered crystals. Transition metal trichalcogenides MX₃, where M is transition metal Ti or Zr and X is S, Se or Te, are typical vdW stacked layered materials.¹⁶ Therefore, it is expected that 2D MX₃ nanosheets can be obtained by exfoliating their bulk counterparts.

Experimentally, the electrical and optical properties of bulk TiS₃, ZrSe₃, HfSe₃, ZrS₃ and ZrTe₃ have been studied.¹⁷⁻²¹ Few-layer TiS₃ nanoribbons have been successfully isolated and the macroscopic films of TiS₃ ribbons show a direct band gap of ~1.1 eV and ultrahigh photoresponse.²²⁻²⁴ However, in theoretical respect, previous studies of these materials were limited to the

band structure calculations of bulk ZrSe₃ and ZrTe₃.²⁵⁻²⁸ Until very recently, the electronic structure of TiS₃ monolayer was computed, and an indirect to direct band gap transition from bulk to monolayer was found.²⁹ Before further applying these materials in nano-electronic and optical devices, a more comprehensive study from theoretical aspect would be needed.

In this paper, we systematically study the structural, electronic and optical properties of monolayer MX₃ sheets. The cleavage energies of bulk MX₃ are evaluated to be close to that of graphite, directly demonstrating the feasibility of obtaining 2D MX₃ crystals by exfoliation. Electronic structure calculations show that the trisulfide and triselenide monolayers are semiconductors with band gaps in the range of 0.57-1.90 eV, while the two tritelluride monolayers are metallic. Contrary to TiS₃, the TiSe₃, ZrS₃ and ZrSe₃ monolayers are all indirect gap semiconductors as their bulks and the indirect to direct band gap transition no longer appears. We further find that due to structural anisotropy, all the semiconductors possess highly anisotropic effective masses and conductive properties. Compared to transition metal dichalcogenides, the extra X-X bonds in these trichalcogenides monolayers introduce states far below the Fermi level and tend not to affect the electronic properties of MX₃ significantly. Finally, the good visible/near-infrared light absorption of TiS₃/TiSe₃ monolayer implies their potential applications in nano-optical devices. In addition, the high anisotropy in light absorption of TiS₃ monolayer offers a possibility to fabricate optical waveguide polarizers.

^a Hefei National Laboratory of Physical Science at the Microscale, University of Science and Technology of China, Hefei, Anhui 230026, China, E-mail: jlyang@ustc.edu.cn; Fax: +86 551 63603748; Tel: +86 551 63606408

^b Synergetic Innovation Center of Quantum Information & Quantum Physics, University of Science and Technology of China, Hefei, Anhui 230026, China

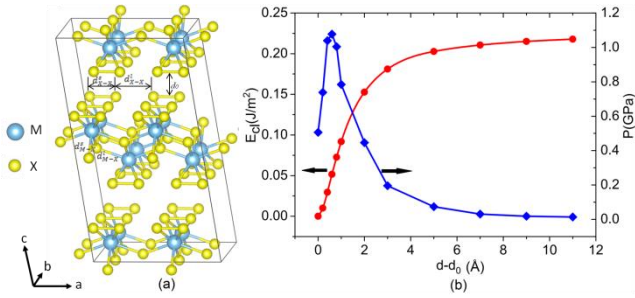


Figure 1. (a) Crystal structure of MX₃ in the ZrSe₃-type structure. Yellow and light blue spheres refer to X (X=S, Se and Te) and M (M=Ti, Zr) atoms. d_{M-X}^s , d_{M-X}^l denote the short and long M-X bonds, d_{X-X}^s , d_{X-X}^l denote the short and long X-X bonds, respectively. (b) Cleavage energy E_{cl} (red) and cleavage strength P (blue) as a function of the separation d between two fractured monolayers.

Table 1. Summary of structural parameters and ideal cleavage cohesion energy (E_{cc}) for monolayer MX₃. (a , b , β), d_{M-X}^s , d_{M-X}^l , d_{X-X}^s , d_{X-X}^l are the lattice constants, short and long M-X bonds, short and long X-X bonds, respectively.

	TiS ₃	TiSe ₃	TiTe ₃	ZrS ₃	ZrSe ₃	ZrTe ₃
a (Å)	4.993	5.328	5.938	5.173	5.450	5.968
b (Å)	3.393	3.538	3.729	3.612	3.740	3.947
β (°)	97.29	97.56	97.55	97.35	97.54	97.77
d_{M-X}^s (Å)	2.491	2.602	2.826	2.622	2.761	2.952
d_{M-X}^l (Å)	2.653	2.843	3.324	2.732	2.892	3.200
d_{X-X}^s (Å)	2.038	2.344	2.821	2.073	2.377	2.855
d_{X-X}^l (Å)	2.956	2.984	3.120	3.101	3.073	3.113
E_{cc} (J/m ²)	0.226	0.376	0.704	0.240	0.373	0.677

Computational Methods

Geometrical optimizations and electronic structure calculations are performed by using the density functional method (DFT) implemented in the Vienna ab initio Simulation Package (VASP).³⁰ The exchange-correlation energy is treated by using the Perdew-Burke-Ernzerhof (PBE) functional, and the Grimme's DFT-D2 dispersion correction³¹ is applied to account for the long-range van der Waals interactions. Since the PBE functional tends to underestimate the band gap of semiconductors, the hybrid HSE06 functional³² is then adopted to get accurate band gaps of single layer MX₃. A vacuum space of ~ 20 Å along the direction normal to the monolayer plane is used so that the interlayer interaction generated by the periodic boundary condition can be neglected. The ion-electron interaction is treated by using the projector-augment-wave (PAW) technique.^{33,34} For geometrical optimization, both lattice constants and atomic positions are relaxed until the forces on the atoms are less than 0.02 eV/Å and the total energy change is less than 1.0×10^{-5} eV. A $7 \times 10 \times 1$ Monkhorst-Pack³⁵ grid and a kinetic energy cutoff of 500 eV are selected. For static calculations, a finer $14 \times 20 \times 1$ grid is chosen.

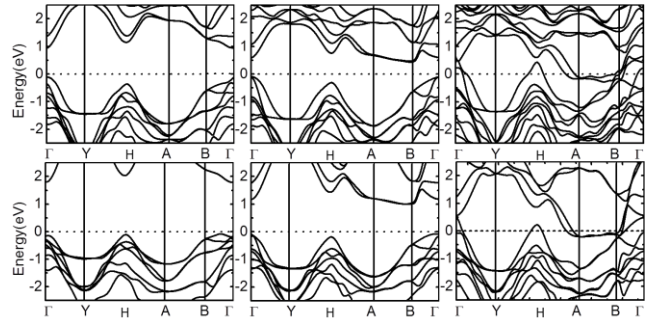


Figure 2. Electronic band structure calculated with HSE06 functional for (a) TiS₃, (b) TiSe₃, (c) TiTe₃, (d) ZrS₃, (e) ZrSe₃ and (f) ZrTe₃ monolayers. The Fermi level is set to zero. Γ (0.0, 0.0, 0.0), Y (0.0, 0.5, 0.0), H (0.25, 0.0, 0.0), A (0.5, -0.5, 0.0), B (0.5, 0.0, 0.0) refer to the special points in the first Brillouin zone.

Results and Discussion

We start our calculations from the benchmarks of the geometrical and electronic properties of bulk TiS₃ to evaluate the accuracy of the methods adopted in this work. The optimized lattice constants of bulk TiS₃ by PBE with Grimme's D2 correction is $a=4.982$ Å, $b=3.392$ Å, $c=8.887$ Å and $\beta=97.24^\circ$, matching well with the experimental values ($a=4.958$ Å, $b=3.401$ Å, $c=8.778$ Å and $\beta=97.32^\circ$).³⁶ The indirect and direct band gaps of bulk TiS₃ calculated with HSE06 functional are 1.02, 1.13 eV respectively. The latter is consistent with the experimentally observed optical band gap of bulk TiS₃ (~ 1 eV^{17,37}), confirming the validity of our methods.

We then turn to the structural properties of MX₃ monolayers. Bulk MX₃ usually crystallize in the monoclinic ZrSe₃-type structure composed of vdW stacked parallel sheets, where one-dimensional chains of triangular MX₃ prisms along the b lattice direction are linked together in the a direction [Figure 1(a)]. Thus, monolayer MX₃ can be viewed as inter-connected one-dimensional chains of triangular MX₃ prisms, with the M-X bonds in the chains being significantly shorter than those between the chains (Table 1). Moreover, different from transition metal dichalcogenides, the structure of MX₃ possesses two types of chalcogen atoms, i.e. outermost X atoms and inner X atoms. The outermost X atoms form X-X chains with alternating bond length d_{X-X}^s and d_{X-X}^l , displaying in Figure 1(a). The structural parameters of the optimized MX₃ monolayers are summarized in Table 1. Clearly we can see the lattice constants expand with the increase of atomic radius, for example, since the atomic radius of Te (Zr) is bigger than that of S (Ti), the lattice constants a and b of TiTe₃ (ZrS₃) are about 18.9% (3.6%) and 9.9% (6.5%) larger than those of TiS₃.

In order to investigate the possibility of obtaining 2D MX₃ monolayers from their bulk crystals, we calculate the ideal cleavage cohesion energy of each material by introducing a fracture in the bulk.³⁸ The variations of total energy according to the separation d between the fractured parts are calculated to simulate the exfoliation procedure. As shown in Figure 1(b), the total energy of TiS₃ increases with d and converges to its ideal cleavage cohesion energy of 0.23 J/m² with a cleavage strength of 1.1 GPa. In the same way, the ideal cleavage cohesion energies of

Table 2. Summary of electronic structure of bulk and monolayer MX₃. The capitals I, D, M indicate the material is an indirect or direct band gap semiconductor, or metal, respectively. Both the values of indirect and direct band gaps E_gⁱ and E_g^d are calculated. M_e^{*} and M_h^{*} are the effective masses of electron and hole along **a** and **b** directions at conduction band minimum and valence band maximum, respectively. The unit is of the electron rest mass (m_{e0}). The density of states (DOS) per chemical formula at the Fermi level for metallic TiTe₃ and ZrTe₃ are also given.

	TiS ₃	TiSe ₃	TiTe ₃	ZrS ₃	ZrSe ₃	ZrTe ₃
Bulk	I	I	M	I	I	M
E _g ⁱ (eV)	1.02/ΓZ	0.21/ΓB	-	1.83/HZ	0.75/ΓB	-
E _g ^d (eV)	1.13/ΓΓ	0.73/ΓΓ	-	2.13/HH	1.29/ΓΓ	-
Monolayer	D	I	M	I	I	M
E _g ⁱ (eV)	-	0.57/ΓB	-	1.90/HΓ	1.17/ΓB	-
E _g ^d (eV)	1.06/ΓΓ	0.70/ΓΓ	-	1.96/ΓΓ	1.28/ΓΓ	-
M _e [*] (m _{e0})						
a	1.47	0.19	-	1.30	0.16	-
b	0.41	4.29	-	0.40	6.72	-
M _h [*] (m _{e0})						
a	0.32	3.57	-	1.28	2.36	-
b	0.98	0.85	-	0.42	0.89	-
DOS(E _F)	-	-	0.91	-	-	1.01

other materials are also evaluated and listed in the last line of Table 1. Here, both the ideal cleavage cohesion energies of TiS₃ and ZrS₃ are smaller than the experimentally estimated cleavage energy in graphite (~0.36 J/m²), and the values of TiSe₃ and ZrSe₃ are very close to that of graphite, which directly demonstrate the feasibility of exfoliation. As with TiTe₃ and ZrTe₃, which possess about twice the cleavage energy of graphite, the exfoliation process would be harder compared to the trisulfides and triselenides.

To study the electronic properties of MX₃ monolayers, the band structures are calculated, as plotted in Figure 2. The obtained band gaps are summarized in Table 2, along with those of bulk crystals for comparison. As we can see, there are three interesting features. First, an indirect to direct band gap transition from bulk to monolayer is found for TiS₃, in accord with the previous study.²⁹ Second, the band gap decreases with the increasing size of the chalcogen atoms, for example, compared with TiS₃, monolayer TiSe₃ possesses a reduced band gap of 0.57 eV, while monolayer TiTe₃ becomes metallic. The same trend is also observed in zirconium trichalcogenides. Last, compared with their bulk counterparts, the indirect band gaps of all monolayers increase, while the direct band gaps decrease. Thus the differences between indirect and direct band gaps of the monolayers become much smaller than the bulk. For example, the disparity between indirect and direct band gaps is 0.3 eV for bulk ZrS₃, while it is reduced to 0.06 eV for monolayer ZrS₃. However, the indirect to direct band gap transition from bulk to monolayer no longer appears.

The effective masses are indicative of the conduction properties of semiconductors. Low effective mass corresponds to high mobility of the electrons/holes and consequently high conductivity. To investigate the conduction properties of semiconducting MX₃ monolayers, we compute the electron and hole effective masses at conduction band minimum (CBM) and valence band maximum (VBM) according to the following equation:

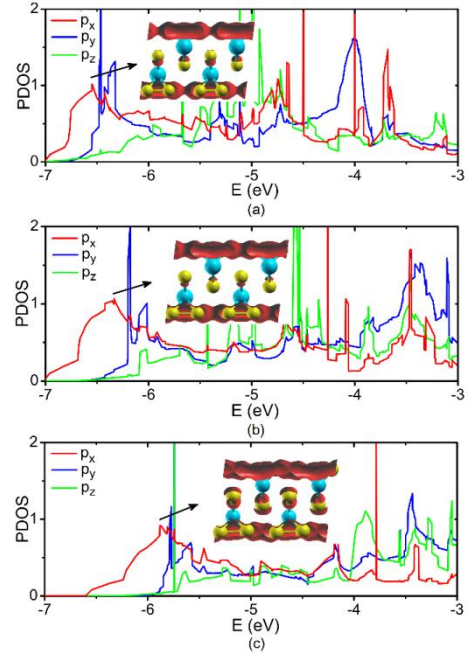


Figure 3. Orbital projected density of states (PDOS) of outermost X atoms in (a) TiS₃, (b) TiSe₃ and (c) TiTe₃ monolayers. The insets are spatial charge plots of the states (viewed along **b** axis) in energy ranges of -7.0 ~ -6.0 eV, -6.8 ~ -5.8 eV, -6.3 ~ -5.3 eV for TiS₃, TiSe₃ and TiTe₃ monolayers, respectively. Isovalues are set to be 0.03 e/Å³. Fermi levels are all set to zero.

$$\frac{1}{m^*(\bar{k})} = \frac{1}{\hbar^2} \frac{\partial^2 E(\bar{k})}{\partial \bar{k}^2}$$

The results are summarized in Table 2. The obtained effective masses are comparable to that of monolayer MoS₂ (M_e^{*} = 0.48m_{e0}, M_h^{*} = 0.64m_{e0}).³⁹ Due to different structural and bonding characters in the **a** and **b** lattice directions, all the materials possess highly anisotropic effective masses for both electron and hole, and the effective masses of triselenide monolayers exhibit larger anisotropy than those of trisulfide monolayers. What's more, except for ZrS₃, the electron and hole effective masses show entirely different anisotropy, i.e. electrons and holes prefer to conduct in different directions. Another interesting finding is that the trisulfides TiS₃ and ZrS₃ have small electron mass in the direction along the chains of triangular MX₃ prisms, namely **b** direction, while for the triselenides TiSe₃ and ZrSe₃, electrons are more easily transported in the **a** direction, which is nearly perpendicular to **b**.

For metallic MTe₃ monolayers, the electrical conductivity is directly proportional to the density of states at Fermi level N(E_F). The calculated N(E_F) of TiTe₃ and ZrTe₃ per chemical formula is 0.91 and 1.01, respectively (Table 2). Comparing with 0.72 states per formula of superconducting MgB₂,⁴⁰ the N(E_F) values of TiTe₃ and ZrTe₃ imply the possibility to achieve 2D superconductivity in these two materials.

Comparing with monolayer transition metal dichalcogenides, monolayer MX₃ trichalcogenides have an additional X-X (X= S, Se, Te) bond. In order to study the effect of this additional X-X bond on the electronic properties, we calculate the orbital-projected density of states of outermost X atoms (Figure 3). One can identify that it is the p_x orbital of outermost X atom that

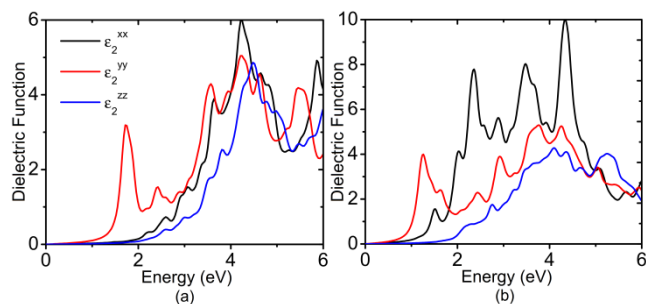


Figure 4. Calculated imaginary part of the frequency-dependent dielectric function $\epsilon_2(E)$ for (a) TiS_3 and (b) TiSe_3 monolayers with HSE06 functional.

contributes to the X-X bonding states, which are far away from the Fermi level. Thus, the additional X-X bonds tend not to affect the electronic properties of MX_3 significantly.

The fact that monolayer TiS_3 has a direct band gap of 1.06 eV, which is very close to the crystalline silicon (~1.1 eV, indirect), indicates that besides potential applications in nano-electronics, monolayer TiS_3 can be also very useful in optical applications, for example, as a solar absorber material. To investigate this possibility, we calculate the imaginary part of the frequency-dependent dielectric function from the summation over pairs of occupied and empty states without considering the local field effects.⁴¹ As shown in Figure 4(a), the imaginary part of the dielectric function shows an anisotropic feature where $\epsilon_2^{xx} \neq \epsilon_2^{yy} \neq \epsilon_2^{zz}$. In particular, ϵ_2^{yy} has a very strong peak at about 1.7 eV, which is due to the interband transition between VB and CB. Because of the dispersion of VB and CB, the optical absorption lasts up to about 2.0 eV. There are also other absorption peaks due to other interband transitions, for example at around 2.4 eV, 3.0 eV and 3.5 eV. Similarly, the dielectric function of TiSe_3 is also computed and shows a strong absorption peak at about 1.2 eV, and other peaks at around 2.4 eV and 3.6 eV [Figure 4(b)]. These results indicate that monolayer TiS_3 is a promising material for absorbing visible light, while TiSe_3 is a good absorber for both near-infrared and visible light.

Remarkably, ϵ_2^{xx} of TiS_3 monolayer is nearly zero at about 1.7 eV while the peak of ϵ_2^{yy} is very high [Figure 4(a)]. This property implies TiS_3 monolayer is a candidate material for designing an optical waveguide polarizer. Polarizer is one of the most important devices in optics, which only transmits the light in one polarization direction by absorbing or reflecting the light in the other polarization direction.⁴² The high anisotropy in optical absorption of TiS_3 monolayer indicates a high polarization sensitivity, and provides a good opportunity for designing optical waveguide polarizers.

Conclusions

In conclusion, based on first-principles calculations, we systematically investigate the structural, electronic and optical properties of titanium and zirconium trichalcogenides monolayer sheets, which can be realized by exfoliating their bulk crystals, as suggested by our estimated low cleavage energies. Similar to MoS_2 , TiS_3 undergoes an indirect to direct band gap transition from bulk to monolayer, while TiSe_3 , ZrS_3 and ZrSe_3 monolayers have indirect band gaps in the range of 0.57 eV-1.90 eV, and the TiTe_3 and ZrTe_3 monolayers are metallic. The calculated electron

and hole effective masses show that all the semiconductors have anisotropic conductive properties. Compared to transition metal dichalcogenides, the extra X-X bonds existed in these trichalcogenides monolayers do not affect the electronic properties significantly. Optical studies reveal that TiS_3 and TiSe_3 monolayers have good optical absorption in the visible and near-infrared region respectively, making them promising in fabricating nano-optical devices. Particularly, the high anisotropy in the light absorption of TiS_3 monolayer makes it a potential material for the design of optical waveguide polarizers.

AUTHOR INFORMATION

Corresponding Author

*jlyang@ustc.edu.cn

ACKNOWLEDGMENT

This work is partially supported by the National Key Basic Research Program (2011CB921404), by NSFC (21421063, 91021004, 21233007), by Chinese Academy of Sciences (CAS) (XDB01020300), and by USTCSCC, SCCAS, Tianjin, and Shanghai Supercomputer Centers.

Notes and references

1. K. S. Novoselov, A. K. Geim, S. Morozov, D. Jiang, Y. Zhang, S. Dubonos, I. Grigorieva, A. Electric, *Sci.*, 2004, **306**, 666.
2. C. Jin, F. Lin, K. Suenaga and S. Iijima, *Phys. Rev. Lett.*, 2009, **102**, 195505.
3. K. K. Kim, A. Hsu, X. Jia, S. M. Kim, Y. Shi, M. Hofmann, D. Nezich, J. F. Rodriguez-Nieva, M. Dresselhaus and T. Palacios, *Nano Lett.*, 2011, **12**, 161.
4. Y. Liu, S. Bhowmick and B. I. Yakobson, *Nano Lett.*, 2011, **11**, 3113.
5. B. Radisavljevic, A. Radenovic, J. Brivio, V. Giacometti and A. Kis, *Nat. Nanotech.*, 2011, **6**, 147.
6. Q. H. Wang, K. Kalantar-Zadeh, A. Kis, J. N. Coleman and M. S. Strano, *Nat. Nanotech.*, 2012, **7**, 699.
7. K. F. Mak, C. Lee, J. Hone, J. Shan and T. F. Heinz, *Phys. Rev. Lett.*, 2010, **105**, 136805.
8. L. Li, Y. Yu, G. J. Ye, Q. Ge, X. Ou, H. Wu, D. Feng, X. H. Chen and Y. Zhang, *Nat. Nanotech.*, 2014, **9**, 372.
9. H. Liu, A. T. Neal, Z. Zhu, Z. Luo, X. Xu, D. Tománek and P. D. Ye, *ACS Nano.*, 2014, **8**, 4033.
10. J. Dai and X. C. Zeng, *J. Phy. Chem. Lett.*, 2014, **5**, 1289-1293.
11. H. Guo, N. Lu, J. Dai, X. Wu and X. C. Zeng, *arXiv preprint arXiv:1403.6209* 2014.
12. V. Tran, R. Soklaski, Y. Liang and L. Yang, *arXiv preprint arXiv:1402.4192* 2014.
13. J. N. Coleman, M. Lotya, A. O'Neill, S. D. Bergin, P. J. King, U. Khan, K. Young, A. Gaucher, S. De and R. J. Smith, *Sci.*, 2011, **331**, 568.
14. J. Feng, X. Sun, C. Wu, L. Peng, C. Lin, S. Hu, J. Yang and Y. Xie, *J. Am. Chem. Soc.*, 2011, **133**, 17832.
15. V. Nicolosi, M. Chhowalla, M. G. Kanatzidis and M. S. Strano, J. N. Coleman, *Sci.*, 2013, **340**, 1226419.
16. W. Krönert and K. Z. Plieth, *Anorg. Allg. Chem.*, 1965, **336**, 207.
17. E. Finkman and B. Fisher, *Solid State Commun.*, 1984, **50**, 25-28.
18. S. Kikkawa, M. Koizumi, S. Yamanaka, Y. Onuki and S. Tanuma, *phys. Status solidi A*, 1980, **61**, K55.
19. I. Gorlova, V. Y. Pokrovskii, S. Zytsev, A. Titov and V. Timofeev, *J. Exp.Theor. Phys.*, 2010, **111**, 298.
20. M. Hoesch, X. Cui, K. Shimada, C. Battaglia, S.-i. Fujimori and H. Berger, *Phys. Rev. B*, 2009, **80**, 075423.

-
21. D. Pacil é M. Papagno, M. Lavagnini, H. Berger, L. Degiorgi and M. Grioni, *Phys. Rev. B*, 2007, **76**, 155406.
 22. J. O. Island, M. Buscema, M. Barawi, J. M. Clamagirand, J. R. Ares, C. Sánchez, I. J. Ferrer, G. A. Steele, H. S. van der Zant and A. Castellanos - Gomez, *Adv. Opt. Mater.*, 2014, **2**, 641.
 23. I. Ferrer, M. Maci á V. Carcel án, J. Ares and C. Sánchez, *Energy Procedia*, 2012, **22**, 48.
 24. I. Ferrer, J. Ares, J. Clamagirand, M. Barawi and C. Sánchez, *Thin Solid Films* 2013, **535**, 398.
 25. D. Bullett, *J. Phys. C.*, 1979, **12**, 277.
 26. H. Myron, B. Harmon and F. Khumalo, *J. Phys. Chem. Solids*, 1981, **42**, 263.
 27. K. Stöwe and F. R. Wagner, *J. Solid State Chem.*, 1998, **138**, 160.
 28. C. Felser, E. Finckh, H. Kleinke, F. Rocker and W. Tremel, *J. Mater. Chem.*, 1998, **8**, 1787.
 29. J. Dai and X. C. Zeng, *arXiv preprint arXiv:1501.02313* 2015
 30. G. Kresse and J. Furthmüller, *Phys. Rev. B*, 1996, **54**, 11169.
 31. S. Grimme, J. Antony, S. Ehrlich and H. Krieg, *J. Chem. Phys.* 2010, **132**, 154104.
 32. J. Heyd, G. E. Scuseria and M. Ernzerhof, *J. Chem. Phys.*, 2006, **124**, 219906.
 33. P. E. Blöchl, *Phys. Rev. B*, 1994, **50**, 17953.
 34. G. Kresse and D. Joubert, *Phys. Rev. B*, 1999, **59**, 1758.
 35. H. J. Monkhorst and J. D. Pack, *Phys. Rev. B*, 1976, **13**, 5188.
 36. S. Furuseth, L. Brattas and A. Kjekshus, *Acta Chem. Scand.*, 1975, **29**, 623.
 37. L. Brattas and A. Kjekshus, *Acta Chem. Scand.*, 1972, **26**, 3441.
 38. X. X. Li, X. Wu and J. L. Yang, *J. Am. Chem. Soc.*, 2014, **136**, 11065.
 39. W. Yun, S. Han, S. Hong, I. Kim and J. Lee, *Phys. Rev. B*, 2012, **85**, 033305 .
 40. J. Kortus, I. Mazin, K. Belashchenko, V. Antropov and L. Boyer, *Phys. Rev. Lett*, 2001, **86**, 4656.
 41. H. Xiang, Z. Huang, Z. Li, S. Wei, J. L. Yang and X. Gong, *Phys. Rev. X*, 2012, **2**, 011003.
 42. R. Sinha and Y. Kalra, *Opt. Express*, 2006, **14**, 10790.
-